Earth's Future

RESEARCH ARTICLE
10.1029/2023EF004257

Special Collection:
Advancing Interpretable AI/ML Methods for Deeper Insights and Mechanistic Understanding in Earth Sciences: Beyond Predictive Capabilities

Spatiotemporal Variability of Channel Roughness and its Substantial Impacts on Flood Modeling Errors

Md Abdullah Al Mehedi[1], Shah Saki[2], Krutikkumar Patel[3], Chaopeng Shen[4], Sagy Cohen[5], Virginia Smith[1], Adnan Rajib[3], Emmanouil Anagnostou[2], Tadd Bindas[4], and Kathryn Lawson[4]

[1]Department of Civil and Environmental Engineering, Villanova University, Villanova, PA, USA, [2]Department of Civil and Environmental Engineering, University of Connecticut, Storrs, CT, USA, [3]Department of Civil Engineering, University of Texas, Arlington, TX, USA, [4]Department of Civil and Environmental Engineering, The Pennsylvania State University, University Park, PA, USA, [5]Department of Geography and the Environment, The University of Alabama, Tuscaloosa, AL, USA

Abstract Manning's roughness coefficient, *n*, is used to describe channel roughness, and is a widely sought-after key parameter for estimating and predicting flood propagation. Due to its control of flow velocity and shear stress, *n* is critical for modeling timing of floods and pollutants, aquatic ecosystem health, infrastructural safety, and so on. While alternative formulations exist, open-channel *n* is typically regarded as temporally constant, determined from lookup tables or calibration, and its spatiotemporal variability was never examined holistically at large scales. Here, we developed and analyzed a continental-scale *n* dataset (along with alternative formulations) calculated from observed velocity, slope, and hydraulic radius in 200,000 surveys conducted over 5,000 U.S. sites. These large, diverse observations allowed training of a Random Forest (RF) model capable of predicting *n* (or alternative parameters) at high accuracy (Nash Sutcliffe model efficiency >0.7) in space and time. We show that predictable time variability explains a large fraction (~35%) of *n* variance compared to spatial variability (50%). While exceptions abound, *n* is generally lower and more stable under higher streamflow conditions. Other factorial influences on *n* including land cover, sinuosity, and particle sizes largely agree with conventional intuition. Accounting for temporal variability in *n* could lead to substantially larger (45% at the median site) estimated flow velocities under high-flow conditions or lower (44%) velocities under low-flow conditions. Habitual exclusion of *n* temporal dynamics means flood peaks could arrive days before model-predicted flood waves, and peak magnitude estimation might also be erroneous. We therefore offer a model of great practical utility.

Plain Language Summary Stream channel roughness is a critical variable for many river-related applications including modeling of flood inundation extent, pollutant transport, stormwater management, aquatic ecosystem health, infrastructural safety, and so on, and is traditionally assumed as being constant over time. Here we estimate channel roughness using in-stream measurements from thousands of sites across the United States and show that its temporal dependence can be substantial. Our machine learning model can serve as a valuable and state-of-the-art prediction of roughness, providing great practical value and a holistic view of the spatiotemporal variability of roughness. Moreover, the longstanding exclusion of temporal dynamics means that flood peaks could arrive days before model-predicted flood waves, and peak magnitude estimation might also be inaccurate. Raising awareness of this issue can advance our understanding of channel flows, improve the accuracy of modeling, and save lives.

Key Points:

- We developed a continental-scale dataset of Manning's channel roughness values and trained accurate random forest models to predict them
- Predictable time variability explains a large fraction (~35%) of variance in Manning's roughness compared to spatial variability (50%)
- Ignoring temporal dynamics means flood peaks could arrive days before predicted, and peak magnitude estimation might also be erroneous

Supporting Information:

Supporting Information may be found in the online version of this article.

Correspondence to:

C. Shen, S. Cohen and V. Smith,
cshen@engr.psu.edu;
sagy.cohen@ua.edu;
virginia.smith@villanova.edu

Citation:

Al Mehedi, M. A., Saki, S., Patel, K., Shen, C., Cohen, S., Smith, V., et al. (2024). Spatiotemporal variability of channel roughness and its substantial impacts on flood modeling errors. *Earth's Future*, *12*, e2023EF004257. https://doi.org/10.1029/2023EF004257

Received 21 NOV 2023
Accepted 10 JUN 2024

Author Contributions:

Conceptualization: Md Abdullah Al Mehedi, Chaopeng Shen, Sagy Cohen
Data curation: Md Abdullah Al Mehedi, Shah Saki, Krutikkumar Patel
Formal analysis: Md Abdullah Al Mehedi, Chaopeng Shen

1. Introduction

Stream channel roughness, represented by Manning's roughness coefficient (*n*) (Manning et al., 1890), describes the frictional resistance exerted by channel beds, banks, and floodplains to streamflow, and is widely sought-after as a key parameter for estimating and predicting river flow and making river management decisions (Arcement & Schneider, 1989; Dingman & Sharma, 1997; Einstein & Barbarossa, 1952; Mabbott & Fryirs, 2022; Singh, 2017). Given the same flow rate and channel geometries, channels with larger *n* can manifest larger flow depths, slower flows, and more inundation in the surrounding floodplains (Allen et al., 2018; Attari et al., 2021; Heldmyer et al., 2022; Hu et al., 2021; Ji et al., 2019; H.-Y. Li et al., 2015; Lin et al., 2019; Shen et al., 2016; Waliser & Guan, 2017; Yamazaki et al., 2011), while those with low *n* values facilitate faster flood convergence

Investigation: Md Abdullah Al Mehedi, Shah Saki, Krutikkumar Patel, Chaopeng Shen, Sagy Cohen
Methodology: Md Abdullah Al Mehedi, Chaopeng Shen
Resources: Tadd Bindas
Software: Md Abdullah Al Mehedi, Tadd Bindas
Supervision: Md Abdullah Al Mehedi, Chaopeng Shen, Sagy Cohen
Validation: Chaopeng Shen, Sagy Cohen, Virginia Smith, Adnan Rajib, Emmanouil Anagnostou
Visualization: Md Abdullah Al Mehedi, Shah Saki, Krutikkumar Patel, Kathryn Lawson
Writing – original draft: Md Abdullah Al Mehedi, Shah Saki, Chaopeng Shen
Writing – review & editing: Md Abdullah Al Mehedi, Shah Saki, Chaopeng Shen, Sagy Cohen, Virginia Smith, Adnan Rajib, Emmanouil Anagnostou, Kathryn Lawson

downstream. Due to its relationship with flow velocity and shear stress, n is critical for modeling flood timing and other applications (Hilker et al., 2009; Kundzewicz et al., 2018; Rowiński et al., 2022). For example, in river hydrology, n plays a crucial role in modeling the timing of flood peaks and inundation extent, or inverse estimation of discharge (Durand et al., 2016) with biases in n leading to large prediction errors (Ardıçlıoğlu & Kuriqi, 2019; Azamathulla & Jarrett, 2013; Ye et al., 2018). In water quality modeling, river flow speed is critical to calculating pollutant transport. In erosion control and fluvial geomorphology, n is an important control for bank and soil erosion (Langendoen & Simon, 2008). In infrastructural engineering design, n influences the estimation of flow depth (Arcement, 1989) and thus the design criteria of, for example, bridges and culverts (Richardson & Davis, 2001; Yaryan Hall & Bledsoe, 2023). In aquatic ecosystem management, Manning's n is used to design plans for river restoration (Clilverd et al., 2016) and model suitable fish habitat (Fitz et al., 1996; Gillenwater et al., 2006). Therefore, considerable practical and scientific value exists in the robust estimation of n, and there are potential costs of uncertainty in estimation of n.

Until now, limitations in the scale of available datasets have created knowledge gaps in understanding how much and how fast n varies in space and time, and to what extent it is predictable as a function of in-stream and macroscopic environmental factors (Addy & Wilkinson, 2019; Green, 2005; Pradhan & Khatua, 2018a, 2018b; Zhu et al., 2020). In standard engineering practice, roughness is overwhelmingly either determined from published tables summarizing data on land cover, stream order, geomorphology, riverbed materials, vegetation, and so on (where the raw data for such look-up tables are rarely available) or calibrated through matching simulations of flow velocity or volumetric discharge to observations (Arcement, 1989; Rajib et al., 2020). Due to the need for local investigation or calibration, either approach would preclude the estimation of n at large scales. In research, it is understood that channel roughness can be governed by multiple environmental factors including the type and size of the river substrate, channel geometries, flow conditions, sediment characteristics, human modifications, aquatic and riparian vegetation, and plant type and density (Addy & Wilkinson, 2019; Brebbia, 2011; Djajadi, 2009; Jarrett, 1985; Nicosia & Ferro, 2023; Salleh et al., 2023; Zhu et al., 2020). In meandering channels, the irregularity of channel geometry and sinuosity (Figure S1 in Supporting Information S1) can also play a role in determining n (James, 1994; Naghavi et al., 2023). Nevertheless, past studies have mostly focused on a certain type of stream or a limited number of sites (Bhusal et al., 2022; Mehedi et al., 2022; Mohanta et al., 2018; Roushangar & Shahnazi, 2021; Yang et al., 2021), and a large dataset is lacking to enable large-scale Machine Learning (ML) studies of n that would provide holistic and systematic perspectives. Since all these channel properties covary, we hypothesize that catchment area or discharge as integrative signals, along with local environmental predictors, could present a pathway toward better determination of n at large scales.

In current practices and guidelines, n is predominantly viewed as a temporally constant (but often spatially varying) parameter in the mindsets of scientists and engineers (Garrote Revilla et al., 2021; Mangukiya & Yadav, 2022; Vashist & Singh, 2022). Table S1 in Supporting Information S1 provides some example values. Manning's formula with the uniform flow assumption (Equation 1 in Methods) is the most commonly used (Jarrett, 1985; Y. Li et al., 2014; Noarayanan et al., 2012). Although the use of "hydraulic radius" (flow area divided by the wetted perimeter, often approximated by river depth for wide rivers) in Manning's equation is intended to, in theory, remove the dependence of n on discharge, it has not been shown that such discharge-independence truly holds. In fact, some field studies, especially those from the geomorphological community, recognize that Manning's roughness is a function of discharge and that flow resistance tends to be overestimated at high flows (Chow, 1959; Ferguson, 2007, 2010; Ye et al., 2018). Some studies have questioned the validity of the Manning's formula, with alternatives such as Chezy or Keulegan (1938) formulations proposed to address some of the discharge dependency issues (Ferguson, 2010). However, the empirical datasets remain small in number and, more importantly, it is unclear how to leverage the sampled dynamical relationship for predictive purposes. Since flow velocity is inversely proportional to n, if temporal variability is substantial then current models risk significantly miscalculating velocity for extremely high or low flows.

We utilized the large United States Geological Survey (USGS) HYDRoacoustic dataset which supports the Surface Water Oceanographic Topography (HYDRoSWOT) satellite mission (Canova et al., 2016), to provide new insights into the n distribution at large spatiotemporal scales. Compiled from USGS Acoustic Doppler Current Profiler (ADCP) measurements, HYDRoSWOT contains, among other attributes, discharge, flow velocity, and flow depths for over 200,000 observations from thousands of sites across the United States. We derived n using Manning's equation and verified its physical significance utilizing a set of hypothesis tests (see Methods), analyzed its spatiotemporal distributions, and explored its temporal variability. We investigated the following questions.

Table 1
Descriptions of Data Sources

Data	Source	Data type	Coverage
Velocity, channel width, channel depth, discharge	USGS HYDRoSWOT (Canova et al., 2016)	Point	CONUS
Drainage area, stream order, slope, mean elevation	National Hydrography Dataset (U.S. Geological Survey, 2023)	Polylines	CONUS
Land cover, sinuosity, stream density	Wieczorek et al., 2018 (Schwarz et al., 2018b)	Polylines	CONUS
Channel bed particle size (D_{50})	Abeshu et al., 2022 (Abeshu et al., 2022)	Polylines	CONUS
NDVI	MOD13Q1 V6.1 (Didan, 2015)	Raster	Global/250 m
Sand, clay, silt	Hengl et al., 2018 (Hengl, 2018)	Raster	Global/250 m
Aridity index	Trabucco & Zomer, 2019 (Global Aridity Index and Potential Evapotranspiration (ET0) Climate Database V2, 2019)	Raster	Global/250 m

Q1: Given a comprehensive dataset of continental-scale Manning's roughness coefficient *n* (and other flow resistance parameters), can *n* be well predicted by machine learning methods with integrative environmental inputs such as upstream catchment area, along with local environmental conditions, and if so, which attributes are more important predictors and does *n* have significant geographic patterns?

Q2: At the continental scale, how much variance in *n* is due to temporal variation in discharge, in comparison to its spatial variability, and how well can *n* be predicted if discharge is used as an input?

Q3: How many errors in flood peak modeling will be encountered if the temporal variation of *n* is not considered?

2. Materials and Methods

2.1. Datasets

The raw data used in this work (Table 1 in Supporting Information S1) were collected from many global scale research initiatives (Canova et al., 2016; Google Earth Engine, 2023; NHD Plus - NHDPlus Version 2, 2023; Schwarz et al., 2018a). The United States Geological Survey (USGS) compiled HYDRoSWOT, the HYDRo-acoustic dataset in support of the Surface Water Oceanographic Topography satellite mission (Canova et al., 2016), which contains over 200,000 Acoustic Doppler Current Profiler (ADCP) surveys from thousands of sites across the United States. ADCP uses sound waves to measure the speed and direction of currents throughout the water column. Moving-boat ADCPs can produce two-dimensional velocity grids (all three directional velocity components) as well as depth profiles upon completion of a transect. Taking the cross product of the horizontal velocity vectors and the boat's track and integrating over the transect can produce discharge. ADCP surveys can miss a portion of flow above the sensors and portions of the flow close to the banks, but the flows in these portions can be estimated. In HYDRoSWOT, the transect-integrated discharge, mean velocity, maximum depth, and measured width (length of the transect, not necessarily the true river width) are reported. Mean depths were reported only about one third of the time. There are 5,228 total sites, with 67,433 observations. Median characteristics of the sites in the dataset include channel width (28.4 m), maximum depth (1.22 m), drainage area (4.55 km^2), and mean velocity (0.44 m/s).

The Moderate Resolution Imaging Spectroradiometer (MODIS) instrument on the Terra and Aqua satellite missions provides a product (MOD13Q1 V6.1) consisting of Normalized Difference Vegetation Index (NDVI) information, which is referred to as the continuity index to the existing National Oceanic and Atmospheric Administration-Advanced Very High-Resolution Radiometer (NOAA-AVHRR) derived NDVI (Didan, 2015). Sand and clay content data were obtained as percentages (kg/kg) at 6 standard depths (0, 10, 30, 60, 100, and 200 cm) (Hengl, 2018), but only depths of 0 and 10 cm were considered for this study. Aridity Index (AI) represents the ratio between precipitation and evapotranspiration (aggregated on an annual basis) and was obtained from the Global Aridity Index Version 2 dataset (Global Aridity Index and Potential Evapotranspiration (ET0) Climate Database V2, 2019). This dataset provides high-resolution global raster climate data related to evapotranspiration processes and rainfall deficit for potential vegetative growth. Slope was determined using the National Hydrography Dataset version 2 (NHDPlus V2) and averaged for each reach. Therefore, slope was treated as a temporally constant parameter. This assumption is commonly employed in large-scale hydrological and

hydraulic modeling due to the relatively stable nature of physical riverbed features, including slope, over short to medium time scales. However, we acknowledge the potential limitations of assuming a time-constant slope. Specifically, in regions with minimal elevation change, such as coastal rivers, the water surface slope is a critical factor influencing flow velocity. Also, this assumption may introduce errors in modeling areas where backwater flows significantly alter hydraulic conditions. In these contexts, variations in water level due to tidal influences, storm surge, or anthropogenic changes can significantly alter the effective slope and, consequently, the flow dynamics. The assumption of a time-constant slope in such settings could introduce inaccuracies in flood modeling, potentially specifically affecting the precision of predictions in coastal rivers.

Median streambed particle size (D50) across the rivers in the conterminous United States (CONUS) was also used as an input variable (Abeshu et al., 2022). All the input datasets and their sources are listed in Table 1.

2.2. Manning's *n* Calculation

The channel roughness coefficient (n) is derived from Manning's equation for uniform flow in open channels (Singh, 2017):

$$n = \frac{k\,R^{2/3}S^{1/2}}{\mathrm{v}} \tag{1}$$

where R is the hydraulic radius (m), v is the stream velocity (m/s), S is channel slope (m/m), and k is a unit conversion factor that is 1.0 if using v and R in meters, and 1.49 if using feet, leading to the same n value under different unit systems.

To apply Equation 1, R and v were obtained from the transect-average values in the HYDRoSWOT dataset ADCP surveys and S was derived from the NHDPlus V2 dataset (reach averaged). R, v, and thus n are different for different sampling locations as well as time points, but S is only considered site-specific and not time-dependent.

Assuming the channel cross-sectional geometry to be rectangular, R was approximated by the observed maximum depth. We used this value for R for several reasons. First, the majority of the rivers in the dataset are wider than 10 m. Second, during our quality control check, we found that the width value in HYDRoSWOT is deemed less reliable than depth as the surveys may not cover the entire cross section (perhaps due to navigational difficulties or transects not perpendicular to flow), for example, we found max-Q width to be sometimes smaller than that min-Q width, an issue which never occurred with depth. Third, to examine the impact of this assumption on our conclusions, we ran sensitivity tests where either triangular or trapezoidal geometry (bottom width was then solved from flow area) was assumed, and we calculated metrics that quantified the impacts of n variability on estimated velocity (see *Quantifying the Implications* section below). We found the geometric assumption to have little impact on this variability metric or the main conclusions of the paper, as shown in Figure S4 in Supporting Information S1. Finally, our hypothesis testing and analysis all suggest that the n values we calculated have physical significance.

2.3. Input Feature Preparation

Exploratory Data Analysis was performed to obtain insights on the dataset by summarizing its main attributes. We primarily did this to trim the outliers and decide on the transformation function to increase the normality and bivariate correlation of the variables. Based on previous literature and guidelines for the selection of Manning's n, we trimmed the n values to be less than 0.33 (Arcement, 1989). Feature Engineering in this work involved data transformation, data standardization, and splitting the dataset into training/testing sets. A few input variables (e.g., land cover, soil contents, sinuosity) were transformed using logarithmic functions to obtain the most suitable format in order for the learning algorithm of the ML-based regressors to obtain the highest performance. In this study, a tabular dataset was utilized to quantify the percentage of land cover classes within the conterminous United States. This dataset leverages data from the 2011 National Land Cover Dataset (NLCD 2011) and compiles the percentage of land cover classes into two distinct spatial components of the NHDPlus version 2 (NHDPlusv2) data suite (Homer et al., 2015). These components encompass (a) individual reach catchments and (b) accumulated reach catchments upstream through the river network. The inclusion of a unique identifier, COMID, facilitated the linking of this dataset to the NHDPlusv2 data suite. Similarly, information on flowline reach sinuosity was compiled along the flowline NHDPlusv2 COMID data. Through the data standardization

process, the values of the variables were rescaled and centered around their mean with a unit standard deviation. The standardized variables were split into three portions: training (to train the model), validation (to improve the performance of the models through hyperparameter tuning), and testing (to test/evaluate the model performance with unseen data). Seventy percent of the dataset was used for training and the rest was used for validation (15%) and testing (15%). To avoid information leakage, we excluded variables directly involved in calculating n in Equation 1 from the inputs to our models. Selected contributing predictors along with the observed channel roughness were used to train and test the models.

2.4. Machine Learning Model Development

A set of ML-based regressors was chosen for the predictive analysis (Figure S5 in Supporting Information S1), including Random Forest (RF), Multi-layer Perceptron (MLP), Extreme Gradient Boosting (XGB), and K-Nearest Neighbors (KNN). RF is an ensemble learning method for regression operated by constructing a collection of multiple decision trees when training the model (Mehedi et al., 2022). An MLP is a fully connected type of feed-forward neural network (Gaudart et al., 2004). XGB is a distributed gradient-boosted decision tree ML algorithm. KNN is a non-parametric regression method that approximates the association between predictors and the target variable by taking the average of the observations in a similar neighborhood based on a distance function (Song et al., 2017). As the RF model exhibited the top performance among all other regressors with a NSE of 0.7, it was selected for presentation of the results. A grid search cross-validation scheme was used to tune the hyperparameters of the models, taking all the hyperparameter combinations exhaustively (Ippolito, 2022). Spatial k-fold cross-validation was performed for the RF model to measure the model's transferability across terrains (Figure S6 in Supporting Information S1). The entire study domain was clustered into 18 folds according to hydrologic regions, as the spatial autocorrelation among the nearby locations may lead to bias and incorrect model evaluation if the models are evaluated considering the entire study area (de Bruin et al., 2022; Hoffimann et al., 2021). An illustration of the entire process of the k-fold cross-validation is presented in Figure S6 in Supporting Information S1.

The relative feature importance of the predictors was studied by analyzing the Permutation Feature Importance (PFI) technique in the computational domain (Mehedi et al., 2022; Mi et al., 2021). In PFI, the impact of shuffling the values of a feature (e.g., NDVI) over the target variable (e.g., roughness coefficient) is quantified to observe the response in the output variables due to the change in the input variables. The score of the error matrix (R^2) derived from the observed and predicted values of the channel roughness caused by shuffling the predictors provides the score of relative feature importance. A partial dependence plot displays the minimal influence a feature has on a ML model's outcome (Greenwell, 2017), and can demonstrate if a target and a feature have a linear, monotonic, or more complex relationship. The partial dependence plots were calculated after fitting the RF model.

2.5. Variance Decomposition and the Significance of Time Variability

To decompose the spatiotemporal variability of n, we calculated Sum-of-Squares Error (SSE) to quantify the variability. SSE_s is the sum of the squares of the residuals when using the mean n to predict n for a particular site:

$$SSE_s = \sum_s^m \sum_t^{T_s} \left(n_s^t - \overline{n_s}\right)^2 \quad (2)$$

where $\overline{n_s}$ and T_s are, respectively, the mean of calculated n and total number of measurements at site s, n_s^t represents calculated n at time t, and m is the total number of sites. SSE_{RF} shows the RF performance with the original spatiotemporally varying n as an input:

$$SSE_{RF} = \sum_s^m \sum_t^{T_s} \left(n_s^t - RF\left(Q_s^t, x_s\right)\right)^2 \quad (3)$$

SSE_A denotes the total sum-of-squares of n for all the data, where $\overline{n}$ is the mean n of all data points:

$$SSE_A = \sum_s^m \sum_t^{T_s} \left(n_s^t - \overline{n}\right)^2 \quad (4)$$

Table 2
Perturbation Experiments for Manning's Equation

Formula for n	*NSE*	Comments
$n = (1/v)\, R^{2/3} S^{1/2}$	0.71	
Experiments substituting median values for site-specific ones		
$n = (1/v)\, R^{2/3}\, \overline{S}^{1/2}$	0.43	
$n = (1/v)\, \overline{R}^{(2/3)}\, \overline{S}^{(1/2)}$	0.26	
$n = (1/\overline{v})\, R^{2/3}\, \overline{S}^{(1/2)}$	0.21	
$n = (1/\overline{v})\, \overline{R}^{2/3}\, S^{1/2}$	0.18	
$n = (1/v)\, \overline{R}^{2/3}\, S^{1/2}$	0.02	
$n = (1/\overline{v})\, R^{2/3}\, S^{1/2}$	0.11	
Control experiments with an altered formula		
$n'' = v\, R^{2/3}\, S^{1/2}$	0.16	
$n'' = v\, R^{2/3}\, \overline{S}^{1/2}$	0.09	
Subset of sites with more than 40 data points (333 sites, totaling 24,881 data points). $\underline{X_1}$ and $\underline{X_2}$ denotes alternate input sets with Q^t replaced by Q_{mean} or Q_{max} at a site.		
$N = (1/v)\underline{R}^{2/3}\, S^{1/2}$	0.08	
$n = (1/\underline{v})R^{2/3}\, S^{1/2}$	0.21	
$n_{Qmean} = (1/v)R^{2/3}\, S^{1/2}$	0.59	$\underline{X_1}$: Q^t replaced by Q_{mean} at a site
$n_{Qmax} = (1/v)R^{2/3}\, S^{1/2}$	0.63	$\underline{X_2}$: Q^t replaced by Q_{max} at a site
$n = (1/v)R^{2/3}\, S^{1/2}$	0.34	Predicting deviations from at-a-site mean n.

Note. We modified the terms of n and retrained random forest RF(X) models to predict them. Static covariates were always included in inputs X and, unless noted otherwise, the models had time-dependent discharge Q^t in the inputs. In all equations, v is the stream velocity (m/s), R is the hydraulic radius (m), and S is the channel slope (m/m) for all data points (67,433 points from 5,228 sites). Q represents stream volumetric discharge (m^3/s). Nash–Sutcliffe model efficiency coefficient (NSE) is the amount of variance explained by the model, divided by the total variance. NSE values can be interpreted similarly to R^2. v and R are different for each site and each survey, while S is different for each site. A *bar over a variable* indicates taking the median of all data, and an underlined variable indicates the at-a-site median.

We tested a null hypothesis that the time-dependent variation in n is not significant, and the model explains the variance between the discharge (Q) and n only because of the correlation between Q and velocity (v; velocity is involved in calculating n to train the ML models). To this end, we replaced spatiotemporally-varying discharge, Q^t, in the input of RF model RF(Q^t, x) with at-a-site mean (mean of Q at each individual site) discharge, $\underline{Q}$. In addition, both spatiotemporally-varying R and v were replaced by the at-a-site mean values to ignore their temporal variability. Model predictability due to the changes is tabulated in Table 2.

2.6. Hypothesis Testing

Hypothesis testing was performed to observe the physical significance of n. The null hypothesis ($H_{0,1}$) stated that the measurements used in calculating n were irrelevant to the actual n values. The ML model could therefore only obtain high performance in estimating the calculated n if the v and Q were matched at individual sites, meaning their correlation would be the only reason we found estimative (predictive) power from the ML models. The null hypothesis was further divided into three parts for the factors strongly related to channel roughness, that is, S, R, and v. The first part ($H_{0,1a}$) stated that the measured S did not contribute any information related to the actual n. In the second ($H_{0,1b}$) and third ($H_{0,1c}$) parts, the statements were that the observed R and v, respectively, did not bring information related to the actual n. An F-test was performed to analyze the variance in populations for all parts of the hypothesis. In all cases, the alternative hypotheses were proven true with the statement that the variances were significantly different (true ratio of variances is not equal to 1).

To test the significance of time-dependent variation in n, a null hypothesis was formulated ($H_{0,2}$) stating that the ML models could obtain high performance in predicting the calculated n if the v and Q were matched at a site (in other words, variations in measurements of R at a site did not matter). $R^{2/3}$ was separately calculated using the RF-generated n ($R_{RF}^{2/3}$) and median n ($R_{n50}^{2/3}$). The differences between the original time-dependent $R^{2/3}$ and the measured $R^{2/3}$ ($R_{RF}^{2/3}$ and $R_{n50}^{2/3}$), were calculated:

$$\Delta_1 R^{2/3} = R^{2/3} - R_{RF}^{2/3} \tag{5}$$

$$\Delta_2 R^{2/3} = R^{2/3} - R_{n50}^{2/3} \tag{6}$$

2.7. Quantifying the Implications of the Time Variability of *n*

How far off can velocity estimation be if we do not consider n's temporal variability? To answer this question, we compared the estimated flow velocities using the time-dependent RF model and a static RF model trained on the mean conditions (333 sites with >40 surveys; hydraulic radius taken from observations). We trained a temporally-static model with the mean measured discharge from each site ($\underline{Q}$) along with other covariates (x) of the site as inputs, to calculate n values, defined as $n_{\underline{Q}}^{RF\left(\underline{Q},x\right)}$ at each site. Taking the n from this model as the static value for the site and using observed hydraulic radius (depth), we then made velocity predictions using the Manning's formula (Equation 1) at high flows, $v\left(n_{\underline{Q}}^{RF\left(\underline{Q},x\right)}, R_{maxQ}\right)$ and at low flows, $v\left(n_{\underline{Q}}^{RF\left(\underline{Q},x\right)}, R_{minQ}\right)$. We also computed these velocities based on n values estimated from a time-dependent RF model: $v\left(n_{maxQ}^{RF(Q^t,x)}, R_{maxQ}\right)$ and $v\left(n_{minQ}^{RF(Q^t,x)}, R_{minQ}\right)$. Then the ratio between the two velocities was computed separately for high and low flows for each site:

$$r_{maxQ} = \frac{v\left(n_{maxQ}^{RF(Q',x)}, R_{maxQ}\right)}{v\left(n_{\underline{Q}}^{RF\left(\underline{Q},x\right)}, R_{maxQ}\right)} \tag{7}$$

$$r_{minQ} = \frac{v\left(n_{minQ}^{RF(Q',x)}, R_{minQ}\right)}{v\left(n_{\underline{Q}}^{RF\left(\underline{Q},x\right)}, R_{minQ}\right)} \tag{8}$$

We summarized these two metrics for 333 sites using histograms to aid in interpretation (Figure S3 in Supporting Information S1). Values deviating significantly from 1.0 would suggest that the static model is not suitable for use under extreme conditions.

We also sought a different velocity comparison metric without the use of ML models. To this end, we used the data under min-Q conditions to calculate n_{minQ}, and then applied this value to max-Q conditions to estimate $v(n_{minQ}, R_{maxQ})$ using Manning's formula. Then we compared it to the observed max-Q velocity and computed a ratio:

$$r' = \frac{v_{maxQ}}{v(n_{minQ}, R_{maxQ})} \tag{9}$$

r' values consistently larger than 1.0 would mean that the n derived from min-Q conditions is not applicable to max-Q conditions.

Furthermore, we computed r' under both rectangular (default) and trapezoidal (which also can represent triangular shape if bottom width = 0) channel assumptions. For the trapezoidal shape,

$$A_c = \frac{(w_0 + w_1)\, D_t}{2} \tag{10}$$

where w_0 is the bottom width, w_1 is the top width, and D_t is the height of the trapezoid. As HYDRoSWOT provides A_c, maximum depth D, and top width w_1, we can get

$$w_0 = max\left(\frac{2A_c}{D} - w_1, 0\right) \tag{11}$$

and

$$D_t = \frac{2A_c}{(w_0 + w_1)} \tag{12}$$

for each transect survey. The wetted perimeter P for that survey is

$$P = w_0 + 2\sqrt{D_t^2 + (w_1 - w_0)^2/4} \tag{13}$$

Then, the hydraulic radius can be derived as

$$R = A_c/P \tag{14}$$

As mentioned earlier, we deemed the width measurements to be less reliable than those of depth, and thus mainly used the rectangular assumption. The purpose of this exercise here was to quantify the impacts of different channel geometric assumptions on r' and probe whether our conclusion about n's temporal variability remained robust despite some likely errors in width.

We further used a Muskingum-Cunge (MC) routing model (Bindas et al., 2024) to demonstrate the potential impact of using static n values obtained under mean-Q conditions compared to using those from max-Q

conditions. This experiment quantified the error if measured n values under mean flow conditions were used to simulate flood propagation under a flooding scenario. The MC routing method is a simplified and widely employed routing scheme that considers both mass and momentum conservation, while assuming a simplistic prismatic floodwave shape. We chose the Juniata River basin in central Pennsylvania, USA, with a size of around 5,000 km^2, because this size of a basin could reflect the impact of the riverine flow process. The river network was constructed using the NHDPlus V2 geospatial dataset while the runoff was obtained using a trained deep-learning rainfall-runoff model. The full model setup has been described by Bindas et al. (2024). The n values were obtained from several ADCP sites inside the basin which were simplified into a simple threshold-based assignment of values. Essentially, reaches with a drainage area size of less than 427.26 km^2 were assigned one value, those between 427.26 and 754.50 km^2 were assigned another value, and those below 5,273.62 km^2 were assigned a third value. These values were different for min-Q, mean-Q, and max-Q conditions, and are tabulated in Table S2 in Supporting Information S1. While the impact of n values will depend on the size and hydrology of the basin and channel characteristics, this case here merely serves as a qualitative demonstration of the potential pitfalls of the traditional static view of Manning's n.

3. Results

3.1. Testing the Physical Significance of the Calculated n

Because it is difficult to establish "ground truth" values given alternative n estimates, we started our exercise by examining whether the calculated n values have physical significance and truly represent Manning's roughness. First, if they do, n should vary with environmental covariates (x) in a way that is at least partially consistent with our a priori intuition. We found this to be true with available covariates including catchment area, land cover, channel sinuosity, and so on, and evidence is to be shown in the *Impacts of Control Factors* section below. Second, because that random signal is not predictable by x, *the predictability of the calculated n can only be higher than the sum of its parts if the combination is physically meaningful*. If the combination is meaningful, data for each factor of velocity (v), hydraulic radius (R), and channel slope (S) brings unique information about the geomorphological coevolution of the components of n.

In our "sum-larger-than-parts" tests (see Methods), we found that the calculated n values were more predictable as a function of environmental covariates (x) than the different components of the formula. In other words, the quantity n must be composed of data from one site, at the same time, in the form of the Manning's equation (Equation 1 in Methods) for it to be the most predictable. Every time one of the variables in v, R, or S was replaced by either this variable's global mean value or its at-a-site mean (or median) value, the predictability of the resulting n declined significantly (Table 2). The model's performance, measured as the Nash-Sutcliffe model efficiency coefficient (NSE), was even lower when we replaced two variables (instead of one of them at a time) with their mean values. We also ran a control experiment where n had a similar composition but used v instead of $1/v$ in the formula (Table 2), which resulted in very low predictive power. Based on the earlier argument, Manning's equation produced a quantity with higher physical relevance to the environment than the sum of its parts. In all cases, we rejected the null hypotheses that the calculated n was predictable only because some parts of the n calculation were correlated with the predictors (details in Supporting Information S1) and concluded that the calculated n was physically significant.

Hypothesis tests were conducted to examine the relevance of measurements used in estimating n, designated as ($H_{0,1}$). This hypothesis was partitioned into $H_{0,1a}$, $H_{0,1b}$, and $H_{0,1c}$, each postulating the irrelevance of S, R, and v, respectively. F-tests were applied to check variances related to these components. The ratios of the variances were found to be 1.15 for S, 0.23 for R, and 0.02 for v, with all the p-values being approximately zero. The NSE values from the RF models with randomized S, R, and v values were, respectively, 0.29, −18.20, and −0.38, which shows that the estimative power of the ML model degrades significantly with the random shuffling of the S, R, and v values, and thus n was physically linked to those parameters. Therefore, the hypothesis testing proved that the channel roughness n is a physically significant parameter.

This study investigated the impact of time on variation in n by testing another null hypothesis ($H_{0,2}$) which posited that ML model accuracy in predicting n was unaffected by time-related changes in R measurements. This was examined by comparing the original $R^{2/3}$ against calculated values using RF-derived and median n, leading to the formation of two differentials, $\Delta_1 R^{2/3}$ and $\Delta_2 R^{2/3}$. A two-population F-test on the residuals $\Delta_1 R^{2/3}$ and $\Delta_2 R^{2/3}$ was performed to determine any variation in significance. The alternate hypothesis was proven true with the statement

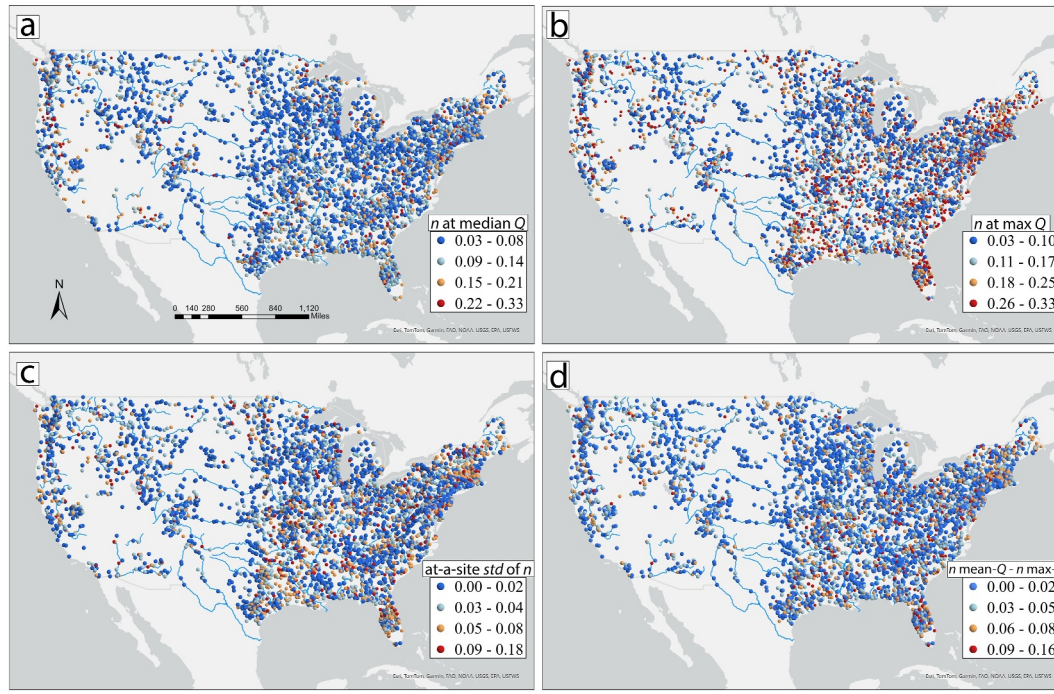

Figure 1. Maps of Manning's n values at (a) median of Q, and (b) maximum of Q at individual sites; (c) standard deviation of n at each site; and (d) the difference between the n values at mean of Q (mean-Q) and maximum of Q (max-Q) at each site. Q is the volumetric streamflow rate (m^3/s).

that the variances were significantly different (true ratio of variances is not equal to 1). The ratios of the variances were found to be 4.83 with all p-values being approximately zero.

3.2. Spatial Distributions of Manning's *n*

The spatial distribution of the calculated n shows no major large-scale gradients for either median- or max-discharge (Q) conditions (Figures 1a and 1b), though several regional patterns (both expected and surprising) stand out. While the pattern of n had been demonstrated previously (Heldmyer et al., 2022), the variability metrics (Figures 1b–1d) have not previously been presented. Generally, low n values are quite prominent over the Great Plains (especially along the major river corridors) and in the Appalachian Plateau (see Figure S2 in Supporting Information S1 for a map of the physiographic provinces of the conterminous USA). High n values are more common along the west coast and parts of the northeastern Appalachian Mountains. While these patterns fit the general description of higher n in mountainous streams, we found a substantial concentration of high n values for streams on the Coastal Plains, especially Florida and southern/coastal Texas. The high n values for these streams could potentially be attributed to backwater flows, pervasive wetlands, and high sinuosity. In addition, there were no clusters of high-n values along the Rocky Mountains, although this could be associated with conditions that do not align with the assumptions of Manning's equation. These patterns counter the general expectation of high values for mountainous regions and low values for flatter regions. Hence, this dataset shows that there may be no geographically simple laws to describe the distribution of n. Similarly, on this scale, there are no clear patterns for the at-a-site temporal standard deviation of n (*std*), other than that *std* tends to be higher where n is also high. However, the noise in n values could partially be due to non-uniform flow conditions (like in coastal zones and reservoirs) for which Manning's equation (with its assumption of uniform flow) does not apply.

The values of n in this dataset are around 0.02–0.05 for the larger rivers and can be as high as 0.33 for some sites. For most of the sites, the n values at mean-Q are larger than the n values at max-Q by ~0.02, but there are also exceptions. These values are on the same order of magnitude as those traditionally reported in the literature. While these results and the small-spatial-scale variability of n are not surprising, this is nonetheless a valuable confirmation that enables us to directly appreciate its spatial distribution.

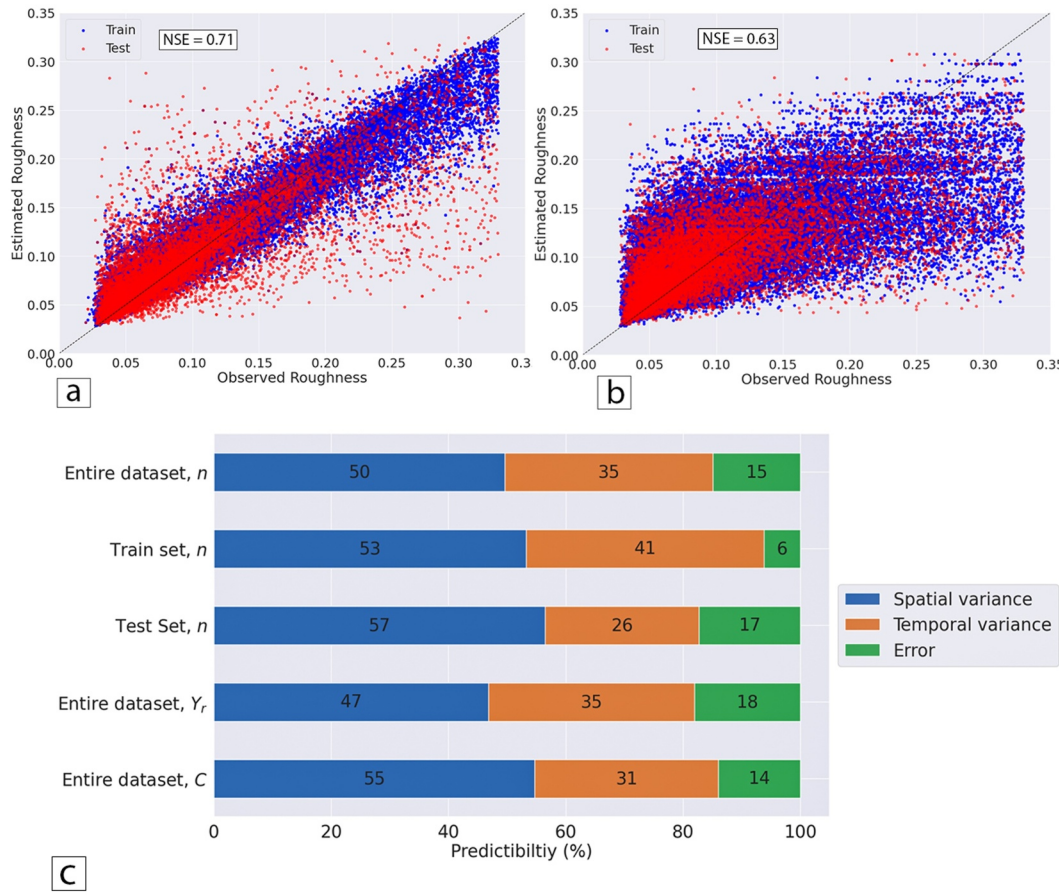

Figure 2. Impact of the spatiotemporal variability of discharge through (a) Random Forest (RF) model performance with the observed discharge as an input, RF(Q^t, x), with Nash-Sutcliffe Efficiency (NSE) of 0.71 (R^2 = 0.7, RMSE = 0.037) and (b) RF(x) model to predict n at maximum discharge at individual sites, with NSE of 0.63. (c) Spatiotemporal variance partitioning of n, C in Chezy's formula and Y_r in Keulegan's form for the entire, training, and testing portions of the dataset using the predictability (%) of the trained RF model. Chezy and Keulegan formulations are described in Equations S1–S3.

3.3. Significance of the Temporal Variability of *n*

Variance decomposition (detailed in Methods) reveals that the predictable time variability explains at least ~35% of the variance of n, in comparison to 50% explained by the spatial variability for all the data points (Figure 2c), which challenges the standard assumption that n is not temporally-variable. The 50% figure comes from the reduction of sum-of-squares of using at-a-site mean n ($\overline{n}^x$) as the prediction (SSE_S) to compute a fraction of the whole variance of n: 1 - SSE_S/SSE_T = 50%. The 35% figure comes from the further reduction in sum-of-squares of residuals of the RF(Q^t, x) model (SSE_{RF}) compared against SSE_S: (SSE_S - SSE_{RF})/SSE_T = 35%. (The notation RF () represents an RF model trained with certain inputs, for example, RF(Q^t, x) uses time-dependent discharge Q^t and temporally-static attributes x to predict the calculated n). The remaining 15% of the variance (SSE_{RF}/SSE_T = 15%) includes unpredictable fluctuations and measurement/calculation noise. Both the training and the testing data suggest a large fraction of variance can be explained by time-dependent discharge (Figure 2).

These fractions of explained variances are somewhat different between the training and testing data, as the RF model inherently performs better for the training data. In our discussion, we quote the 35% figure from all the data points as the overall summary, because the test metric may underestimate the time variability: (a) we may obtain better models, as it is possible that other time-dependent variables also influence n but are not captured by this model; and (b) the RF model cannot fully predict the spatial variance either. Thus, internal to the RF models, the ratio of the temporal to the spatial variance was larger than 31%:51%.

We also calculated alternative formulations of roughness coefficients, including Chezy's C and Y_r from the Keulegan equation (Text S1 and Equations S1–S3 in Supporting Information S1). The RF model performance with C obtained an NSE of 0.74 ($R^2 = 0.74$, RMSE = 11.40), and with Y_r obtained an NSE of 0.68 ($R^2 = 0.68$, RMSE = 2.63). The model performed similarly for all roughness coefficients, with a slightly lower NSE of 0.68 with Y_r. The models with C and Y_r also showed outcomes similar to those obtained with n in terms of variance decomposition. For the entire dataset, the spatial variance accounted for by C was 55% and Y_r was 47%, compared to 50% when using n. The temporal variance remained consistent at 35% for both n and Y_r, whereas it slightly decreased to 31% for C. This result suggests that the Chezy and Keulegan formulations did not offer better resolution of temporal dynamics than n. Our interpretation is that the temporal variation in flow resistance parameters is not entirely due to hydraulic reasons (different flow depths and wetted perimeter), but also depends on changes in channel geometry and channel bed materials. We thus subsequently only focused on n.

To corroborate the importance of temporal variability, we ran hypothesis tests. where (a) we replaced time-dependent discharge (Q^t) in the inputs of RF(Q^t, x) with at-a-site-mean discharge ($\overline{Q}_s$) to get a new model RF ($\overline{Q}_s$, x), which only obtained an NSE of 0.38; and (b) following the predictability argument cited described earlier, we replaced either R or v in the n calculation with its at-a-site-mean values, and the resulting RF models obtained respective NSE values of 0.08 and 0.21 (Table 2). Using at-a-site median values resulted in even lower predictability in both tests (a) (b). These tests suggest the time dependence of n is strong and the various components of n must be combined not only at the same site but also from the same time point for the calculation to be the most meaningful. In all cases, the null hypotheses that time-dependence did not matter were always rejected (details in the Methods and Supporting Information S1). We provide even more velocity-based evidence in the "Discussion" section below.

To offer direct intuition of the time dependence, we visualized how n varies at several sites as a function of discharge and how the RF model captured some of the variation, which showed a diverse range of patterns (Figure 3). At some sites, n declined gradually as discharge increased, either linearly (Figure 3a) or nonlinearly (Figure 3b), and the variation was either well captured by the model (Figures 3a and 3b) or not so well captured (Figure 3e). These figures are consistent with results presented in some earlier work (Ferguson, 2010). However, at some other sites, the n fluctuations at the site were nearly random and uncorrelated with discharge (Figure 3c). At many other sites, n showed a large variability in the low-Q range and trended toward small n values in the high-Q range (e.g., Figures 3d and 3f): therefore the model had to go through the middle of the points. It should be noted that this dataset focuses on the in-channel roughness rather than that of the floodplains. We frequently found all these variations, which were difficult to summarize cleanly. The temporal dependence of discharge seemed to be conditional on other variables, a dependence which the RF model only partially grasped; for example, contrast the declining patterns in Figures 3b and 3d. Different types of variations may be grouped into a few common classes but make identification challenging, and is beyond the scope of this research. The RF model's outputs do not always co-vary smoothly with Q, but the oscillations are generally mild and could be suppressed in the future using monotonicity constraints.

When aggregated by flow percentiles, both the mean value and the variability of n in a flow percentile band were larger for low flow conditions compared to high flows (Figures 4a and 4b). Thus, we may predict n under the peak conditions relatively well. Indeed, a RF model, RF(Q^s_{max}, x), that was given at-a-site maximum discharge (Q^s_{max}) obtained an NSE of 0.63, which was higher than the models for n under mean flow conditions (NSE = 0.36). The larger variability during low flows might be attributed to inherently larger measurement errors as the ADCP sensor used to obtain these data points can only measure a portion of the flow, and a relatively larger portion of the flow would need to be estimated when flow rate is low. Moreover, the bathymetry, flow paths, seasonal vegetation, and human-dependent decisions can vary over several years, which is especially noticeably for low-flow conditions.

3.4. Impact of Control Factors

In our factorial analysis (Permutation Feature Importance, or PFI), discharge was found to have the highest relative importance in estimating Manning's n compared to the other input features, followed by drainage area, land cover factors (e.g., forest cover and agriculture), sinuosity, bed particle size, and so on (Figure 5). The predominant difference between this result and those in the literature is that here, discharge and drainage area are the two most important roles, while they are not explicitly invoked in traditional engineering handbooks, for

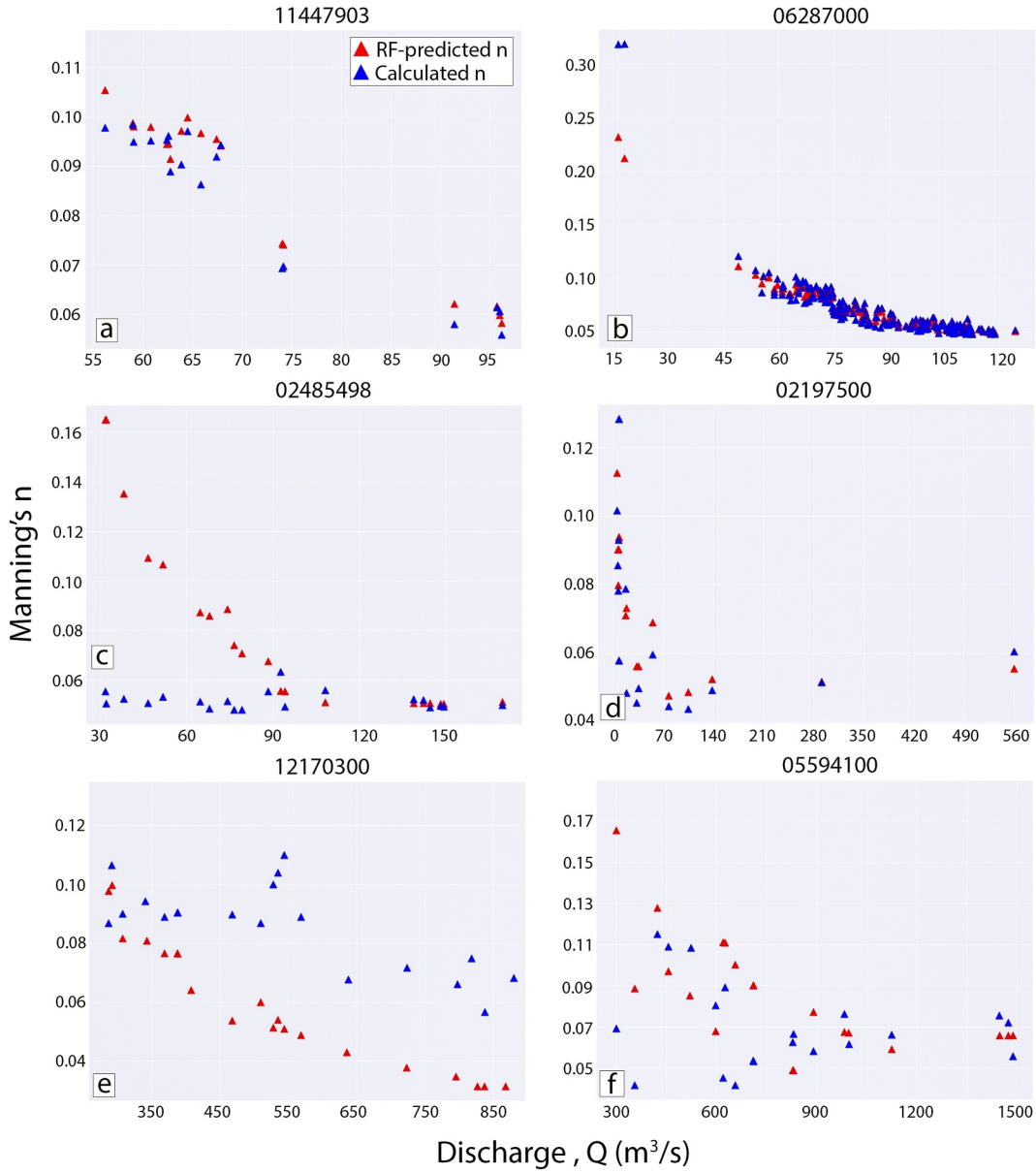

Figure 3. RF model performance in predicting temporally-varying *n* at various sites (a–f) labeled with their USGS monitoring location numbers. Red triangles show the calculated *n* and blue ones show RF-predicted *n*.

example, Water Resources Engineering (third edition) by Larry W. Mays (2019). Based on the variance decomposition analysis, the importance of *Q* comes from both spatial (variation amongst sites) and temporal (variation among measurements taken at the same site over time) influences. The drainage area could have served as a proxy for stream order ("minor" vs. "major" rivers as described in handbooks (Knighton, 1989) or width and depth, which are not easily obtainable from available datasets. As an integrative and more accessible indicator, the importance of catchment area and discharge may mean that there is a pathway toward large-scale prediction of *n* to support flood modeling. The relatively high importance of land cover attributes is partially consistent with the literature, as land cover types are a central defining theme when looking at Manning's *n* lookup tables. However, they are important in the lookup tables only for the floodplains, but here we extracted land cover from a 30-m neighborhood from each site while the *n* dataset likely focused on the in-channel roughness only. The fact that these attributes have reasonably high PFI scores suggests a channel's surrounding land cover may influence (or at least co-vary with) the morphology of the streams. Forests not only evolve with the landscape, but have important

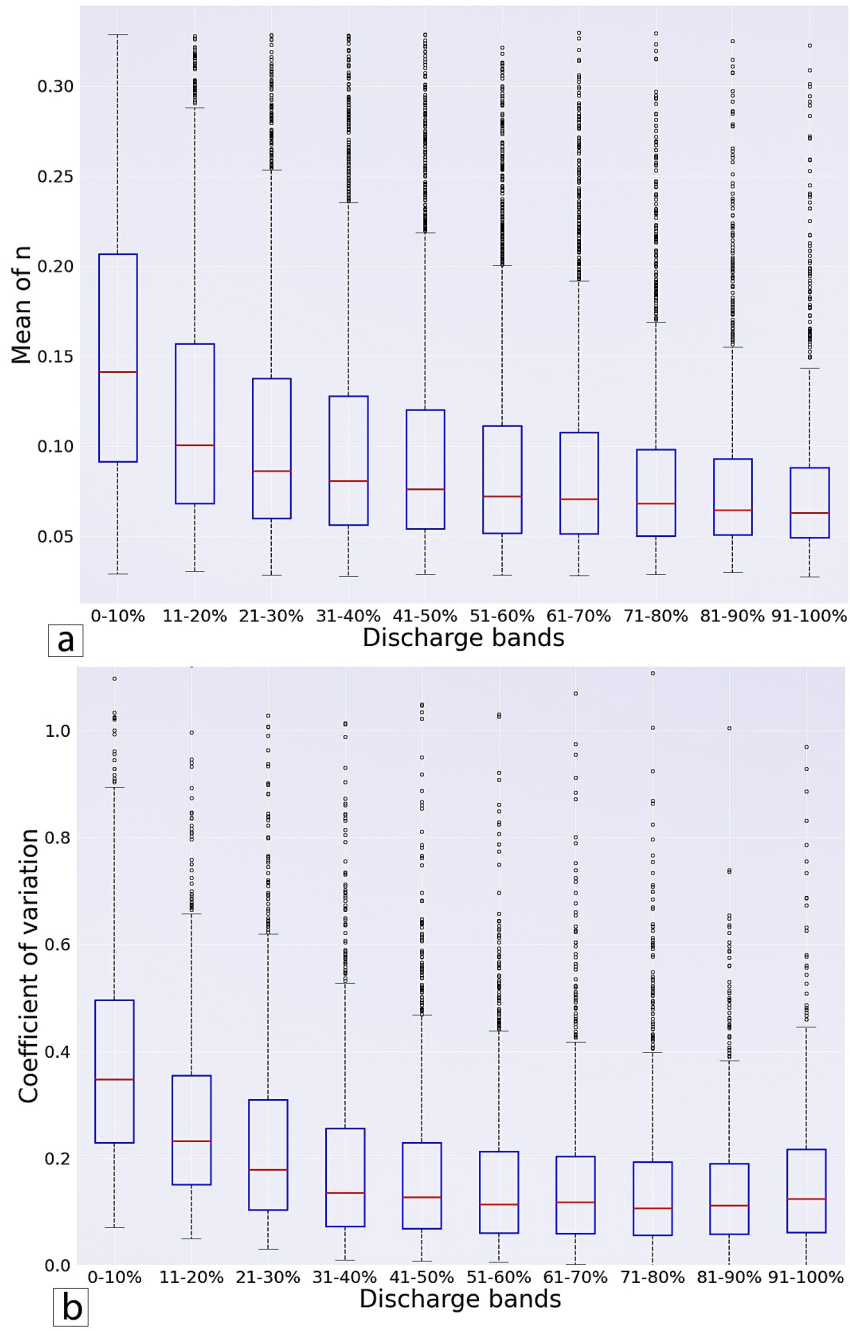

Figure 4. Manning's *n* (a) mean and (b) coefficient of variation (CoV) at all sites for 10 discharge bands (flow percentiles). One set of mean and CoV values was calculated for each site and each flow band, and then those values from different sites were summarized into the boxplots. The horizontal line in each box represents the median, the bottom and top of the box respectively represent the first and third quantiles, and the whiskers extend to 1.5 times the interquartile range from the first and third quantiles.

feedback to the development of the landscape. Except for the streambed mean grain size, Figure 5 shows that the soil attributes are not of great importance. However, this is likely because the data express the soil attributes in a neighborhood, which may have little to do with the streambed materials in nearby streams, or perhaps cannot describe the soil's ability to facilitate bedforms in a manner that impacts flow resistance. Unfortunately, there is no large-scale dataset on bedforms.

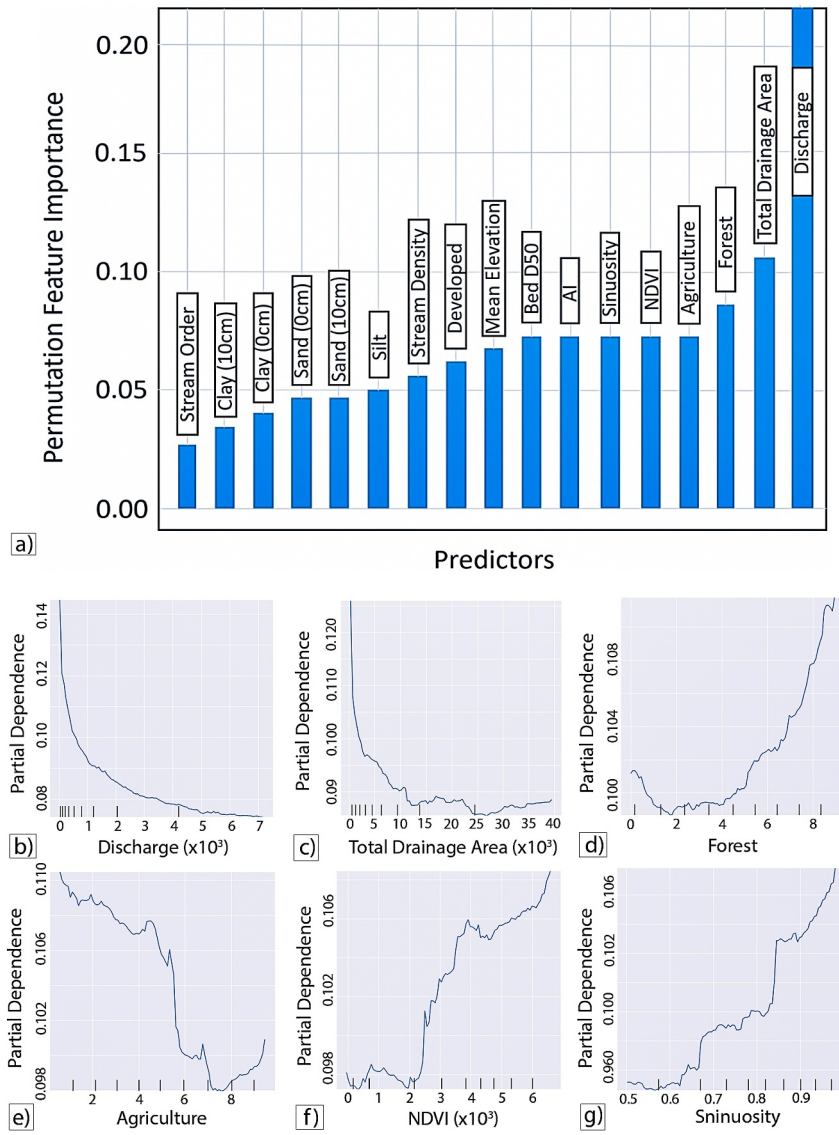

Figure 5. (a) Rank of influencing factors for Manning's *n* according to their feature importance. Here, "AI" stands for aridity index. (b)–(g) Sensitivity of *n* with respect to different external factors with partial dependence response curves. Due to the nature of these curves, the absolute value of the *y*-axis is not very meaningful; the range of the *y*-axis and the shape of the curve are what to focus on. NDVI is Normalized Difference Vegetation Index, which is correlated with vegetation coverage.

While the partial-dependence plots (Figures 5b–5g, essentially an integration of the marginal influence of a single factor) show sensitivities that generally agree with our intuition, it is nonetheless interesting to study these relationships obtained from such a large dataset. The $n \sim Q$ relationship is exhibited by an exponential-decay curve. Drainage area (DA) acts in a similar manner, but separately from Q. Overall, they point to much larger n values for the smaller streams. Higher forest percentage in the neighborhood leads to higher n while agriculture reduces n, but both have a smaller magnitude (0.1–0.11) of influence than either Q or DA. It is well understood that forest cover increases resistance while agricultural land tends to be associated with cleared channel surroundings and straightened channels. Average NDVI (Normalized Difference Vegetation Index), which is correlated with vegetation coverage, is positively correlated with roughness, but can only change n by a small magnitude (0.098–0.106). Sinuosity has a similar impact, and the more sinuous stream tends to have mildly higher n, perhaps due to the impeding effects of meandering and added roughness of deposited materials in the channels.

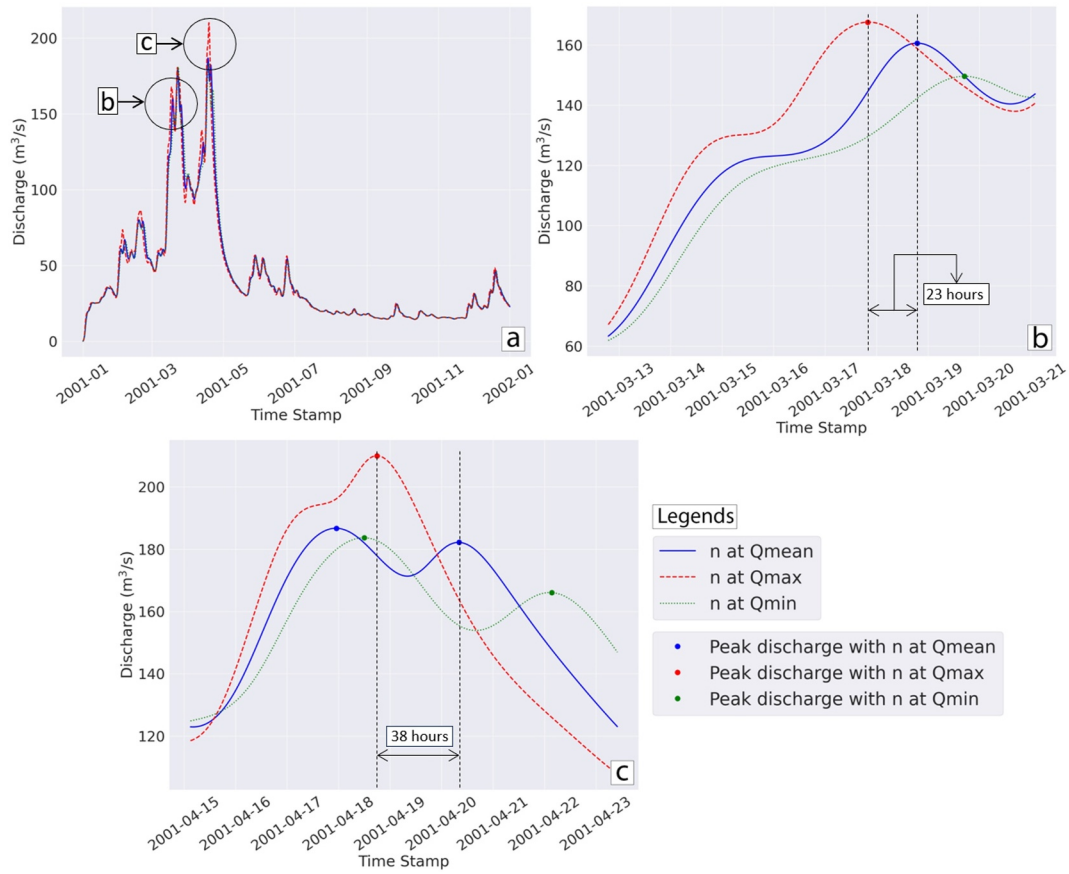

Figure 6. Impact of n values on a standard streamflow routing model (Muskingum-Cunge) in a ~5,000 km^2 watershed in Pennsylvania, USA. (a) Discharge hydrographs for the basin using n values at Q_{mean}, Q_{max}, and Q_{min}. (b) and (c) Close-up views of flow peaks in the hydrographs. Note the differences in both magnitude and time between the predicted peaks depending on which n value was used.

3.5. Implications

The observed n's temporal variability (both mean values and coefficients of variation (CoV) are smaller for high flows) has multifaceted implications regarding how we should measure, estimate, and use n values. First, significant errors could be introduced to large-scale flood and aquatic ecosystem modeling if temporal variability is not considered and if sampling is done at unrepresentative flow conditions. For measured max-Q conditions, the time-dynamic model would produce velocities that are, for the median of 333 sites, 45% higher than the static RF model's results (Figure S3 in Supporting Information S1; details in Methods). Setting aside any machine learning models, the observed max-Q velocity is, at the median, 125% larger than what would be estimated if we applied Manning's formula with n from min-Q measurements ($r' = 225\%$; Figure S4 in Supporting Information S1, details in Methods). Furthermore, it is 135% greater assuming a trapezoidal channel shape instead of rectangular. In contrast, for low flows, the time-dynamic model leads to velocities that are, at the median, 45% lower than the static model's results. Not accounting for the discharge dependence of n, trout habitat modeling efforts, for example, could heavily overestimate the flow velocity.

Errors stemming from the traditional static n could have significant effects on the accuracy of flood modeling. This is demonstrated in a case study for a ~5,000 km^2 watershed in Pennsylvania, USA, where we ran a standard streamflow routing model (Muskingum-Cunge, Figure 6a). The model simulates how the flood wave propagates from upstream to downstream given runoff and river network information. The differences in the flood wave propagations were compared using different sets of n values, obtained under minimum flow, mean flow, and maximum flow conditions (details in Methods). The flood peak using mean-Q n values lags the one with max-Q n values by 23 hr for one of the storm events (Figure 6b), and 36 hr for another larger peak (Figure 6c). This error

could mean that if we used mean-Q in our model, we could have issued a warning for a flood that would be more than a day later than the actual one, and could make the difference between life and death in a real-world situation. Additionally, given n's discharge dependence, the larger the actual peak is, the smaller the max-Q n would be, and the bigger the difference we would see in the timing of the peaks. This dynamic effect also means that even if we calibrated n based on an observed streamflow peak, the calibrated value would not be guaranteed to perform well for other extreme scenarios. Furthermore, since the max-Q n values were much smaller, they led to a smaller gap between two adjacent flood peaks in Figure 6c, and, because of flood wave superposition, a ∼15% higher peak than was simulated using the mean-Q n. This demonstrates that the traditional static approach would produce errors in both flood timing and magnitude, which would not be fixed using a traditional calibration approach with static n values. Similarly, a static model could grossly underestimate pollutant transport speed (thus pollutants could arrive at beaches much earlier than forecasted, resulting in human sickness), or miscalculate impacts on infrastructure and ecosystems.

While the MC routing model was utilized for simulating channel flow, its reliance on kinematic-wave flow routing does incur some limitations. Specifically, the MC model's exclusion of slope dynamics overlooks the feedback loop between channel roughness and flow velocity, where increased roughness leads to reduced velocity and higher water levels. Unlike models that adjust for water surface slope, such as diffusion or dynamic wave models, the MC model's kinematic approach could potentially overestimate the impacts of roughness errors on flow simulations.

3.6. Conclusion

While smaller n values were presented in limited studies in the past, the more predictable n values (within the channel) under high-flow regimes have not been discussed. Decreasing n with higher flow conditions could be explained by a smaller ratio of wetted perimeter to cross-sectional area at high flows, resulting in a weakening viscous effect of riverbed and banks. To account for such dynamic effects, we can either set n to be dynamic, revise Manning's equation to reflect such temporal dependencies, or use a different roughness parameter (though both Chezy's C and Keulegan's Y_r coefficients showed similar results to n). However, judging by the diverse patterns and large errors toward lower discharge, discussed above, it is unlikely that any simple modification to the equation could yield a robust universal model. Therefore, setting n as being dynamic may be a more viable approach for the near future.

Traditional lookup tables of Manning's roughness coefficients focus on local characteristics related to channel bed materials and geomorphology, whereas our study suggests that more attention needs to be paid to basin-scale variables like discharge, catchment area, and sinuosity, which provide integral signals of upstream basin characteristics and are also easier to obtain at large scales. Thus, capable machine learning models (here, NSE>0.7 constitutes a successful model) that utilize widely available geospatial datasets as inputs could arise. It is possible we can refine such future models to be widely applicable at large scales for various applications. Looking forwards, we think there are a variety of possible methods to incorporate the model here into hydraulic models. Long-term Q at different percentiles can be used to update n on a daily or monthly time scale. While this system combining Q and n can be solved simultaneously, the impact may not justify the complexity. It is more likely that we will use a neural network instead of a random forest to support differentiable modeling[88], which can seamlessly connect neural networks to hydraulic models. Then, operator splitting can be employed to calculate n using Q from the last time step, and this n can be used to calculate Q for the present time step.

In this work, we viewed Manning's n as a function of macroscopic environmental variables, while geomorphologists have previously focused on studying it as a physical parameter controlled by grain size, sinuosity, bedload, and so on. Here with the largest dataset and thousands of sites, the time dependency of n and its relevance to the environment are hopefully proven beyond reasonable doubt. The work presented here has revealed a fundamental misconceptualization of river bed roughness, which is of intrinsic interest to water resources engineers and modelers as well as biologists and other scientists studying aquatic ecosystems. Our results show that errors stemming from the traditional temporally-static n could have significant effects on modeling accuracy. Such errors could mean that a flood could arrive a day or more earlier than the forecasted one, with a larger-than-anticipated magnitude, causing otherwise avoidable damages or casualties. It could also mean we underestimate the impacts of floods on bridges, dams, and bank/road erosion, provide mis-timed warnings of river pollutant arrivals to beaches, or miscalculate the available fish habitat after certain perturbations to the hydraulics of a river.

Looking forwards, since neither theory nor data support the concept of a time-constant n, we call for the larger community to start considering Manning's n as being temporally-variable. At the very least, considering the temporal variability of n, we should not use n measured under low flow conditions for flood modeling.

Conflict of Interest

CS and KL have financial interests in HydroSapientInc.a company which could potentially benefit from the results of this research, CS and KL have financial interests in HydroSapient, Inc., a company which could potentially benefit from the results of this research. This interest has been reviewed by the University in accordance with its Individual Conflict of Interest policy, for the purpose of maintaining the objectivity and the integrity of research at The Pennsylvania State University.

Data Availability Statement

All data used for the analysis in this work is publicly available and is cited, respectively. In brief, data on velocity, channel width, channel depth, and discharge are from USGS HYDRoSWOT (Canova et al., 2016). Drainage area, stream order, slope, and mean elevation data are from the National Hydrography Dataset (U.S. Geological Survey, 2023). NDVI data are from the MOD13Q1 V6.1 (Didan, 2015). Soil data, including sand, silt, and clay content, are detailed by Hengl (2018). Aridity index information is from Trabucco and Zomer (2019). Data on channel bed particle size (D50) are taken from Abeshu et al. (2022). The model code developed in this work is available from Al Mehedi (2024).

Acknowledgments
The authors thank the National Oceanic and Atmospheric Administration (NOAA) Office of Water Predictions (OWP) and the National Water Center (NWC) Innovators Program for their support, financial and otherwise, during the 2022 Summer Institute at the NWC and the University of Alabama in Tuscaloosa, Alabama. We thank the anonymous reviewers for their constructive suggestions and comments. This research was initially started and supported by the NWC Summer Institute 2022 at the University of Alabama. The Summer Institute was funded by the National Weather Service and the Consortium of Universities for the Advancement of Hydrologic Science, Inc. (CUAHSI). Chaopeng Shen, Tadd Bindas, and Kathryn Lawson were funded by the National Oceanic and Atmospheric Administration (NOAA) through the Cooperative Institute for Research to Operations in Hydrology (CIROH), award number NA22NWS4320003 with subaward number A22-0307-S003. Sagy Cohen was funded by CIROH subaward number A22-0305. Virginia Smith and Md Abdullah Al Mehedi were supported by the resources from Villanova College of Engineering. Emmanouil Anagnostou and Shah Saki were supported by Eversource Energy Center at UConn. Adnan Rajib and Krutikkumar Patel were funded through the National Aeronautics and Space Administration (NASA) (Grant 80NSSC22K1661).

References

Abeshu, G. W., Li, H.-Y., Zhu, Z., Tan, Z., & Leung, L. R. (2022). Median bed-material sediment particle size across rivers in the contiguous US [dataset]. *Earth System Science Data*, *14*(2), 929–942. https://doi.org/10.5194/essd-14-929-2022

Addy, S., & Wilkinson, M. E. (2019). Representing natural and artificial in-channel large wood in numerical hydraulic and hydrological models. *WIREs Water*, *6*(6), e1389. https://doi.org/10.1002/wat2.1389

Allen, G. H., Pavelsky, T. M., Barefoot, E. A., Lamb, M. P., Butman, D., Tashie, A., & Gleason, C. J. (2018). Similarity of stream width distributions across headwater systems. *Nature Communications*, *9*(1), 610. Article 1. https://doi.org/10.1038/s41467-018-02991-w

Al Mehedi, M. A. (2024). Almehedi06/ManningsRF: Random forest model for continental-scale Channel Roughness estimation (ManningsRF). Large scale prediction of channel roughness coefficient using machine learning. *Zenodo [software]*. https://doi.org/10.5281/zenodo.10945979

Arcement, G. J. (1989). Guide for selecting Manning's roughness coefficients for natural channels and flood plains. https://doi.org/10.3133/wsp2339

Ardıçlıoğlu, M., & Kuriqi, A. (2019). Calibration of channel roughness in intermittent rivers using HEC-RAS model: Case of Sarimsakli creek, Turkey. *SN Applied Sciences*, *1*(9), 1080. https://doi.org/10.1007/s42452-019-1141-9

Attari, M., Taherian, M., Hosseini, S. M., Niazmand, S. B., Jeiroodi, M., & Mohammadian, A. (2021). A simple and robust method for identifying the distribution functions of Manning's roughness coefficient along a natural river. *Journal of Hydrology*, *595*, 125680. https://doi.org/10.1016/j.jhydrol.2020.125680

Azamathulla, H., & Jarrett, R. D. (2013). Use of gene-expression programming to estimate Manning's roughness coefficient for high gradient streams. *Water Resources Management*, *27*(3), 715–729. https://doi.org/10.1007/s11269-012-0211-1

Bhusal, A., Parajuli, U., Regmi, S., & Kalra, A. (2022). Application of machine learning and process-based models for rainfall-runoff simulation in DuPage River basin, Illinois. *Hydrology*, *9*(7), 117. Article 7. https://doi.org/10.3390/hydrology9070117

Bindas, T., Tsai, W.-P., Liu, J., Rahmani, F., Feng, D., Bian, Y., et al. (2024). Improving river routing using a differentiable Muskingum-Cunge model and physics-informed machine learning. *Water Resources Research*, *60*(1). https://doi.org/10.1029/2023WR035337

Brebbia, C. A. (2011). *River basin management VI*. WIT Press.

Canova, M. G., Fulton, J. W., & Bjerklie, D. M. (2016). USGS HYDRoacoustic dataset in support of the Surface Water Oceanographic Topography satellite mission (HYDRoSWOT). *U.S. Geological Survey*. [dataset]. https://doi.org/10.5066/F7D798H6

Chow, V. T. (1959). *Open-channel hydraulics*. McGraw-Hill.

Clilverd, H. M., Thompson, J. R., Heppell, C. M., Sayer, C. D., & Axmacher, J. C. (2016). Coupled hydrological/hydraulic modelling of river restoration impacts and floodplain hydrodynamics. *River Research and Applications*, *32*(9), 1927–1948. https://doi.org/10.1002/rra.3036

De Bruin, S., Brus, D. J., Heuvelink, G. B. M., Van Ebbenhorst Tengbergen, T., & Wadoux, A. M. J.-C. (2022). Dealing with clustered samples for assessing map accuracy by cross-validation. *Ecological Informatics*, *69*, 101665. https://doi.org/10.1016/j.ecoinf.2022.101665

Didan, K. (2015). MOD13Q1 MODIS/Terra vegetation Indices 16-day L3 global 250m SIN grid V006. [dataset]. *NASA EOSDIS Land Processes DAAC*. https://doi.org/10.5067/MODIS/MOD13Q1.006

Dingman, S. L., & Sharma, K. P. (1997). Statistical development and validation of discharge equations for natural channels. *Journal of Hydrology*, *199*(1), 13–35. https://doi.org/10.1016/S0022-1694(96)03313-6

Djajadi, R. (2009). Comparative study of equivalent Manning roughness coefficient for channel with composite roughness. *Civil Engineering Dimension*, *11*(2). Article 2. https://doi.org/10.9744/ced.11.2

Durand, M., Gleason, C. J., Garambois, P. A., Bjerklie, D., Smith, L. C., Roux, H., et al. (2016). An intercomparison of remote sensing river discharge estimation algorithms from measurements of river height, width, and slope. *Water Resources Research*, *52*(6), 4527–4549. https://doi.org/10.1002/2015WR018434

Einstein, H. A., & Barbarossa, N. L. (1952). River Channel Roughness. *Transactions of the American Society of Civil Engineers*, *117*(1), 1121–1132. https://doi.org/10.1061/TACEAT.0006666

Ferguson, R. (2007). Flow resistance equations for gravel- and boulder-bed streams. *Water Resources Research*, *43*(5). https://doi.org/10.1029/2006WR005422

Ferguson, R. (2010). Time to abandon the Manning equation? *Earth Surface Processes and Landforms*, *35*(15), 1873–1876. https://doi.org/10.1002/esp.2091

Fitz, H. C., DeBellevue, E. B., Costanza, R., Boumans, R., Maxwell, T., Wainger, L., & Sklar, F. H. (1996). Development of a general ecosystem model for a range of scales and ecosystems. *Ecological Modelling*, *88*(1), 263–295. https://doi.org/10.1016/0304-3800(95)00112-3

Garrote Revilla, J., González Jiménez, M., et al., Garrote Revilla, J., González Jiménez, M., Guardiola-Albert, C., & Díez Herrero, A. (2021). *The Manning's roughness coefficient calibration method to improve flood hazard analysis in the absence of river bathymetric data: Application to the urban historical zamora city centre in Spain*. MDPI. Retrieved from https://eprints.ucm.es/id/eprint/69759/

Gaudart, J., Giusiano, B., & Huiart, L. (2004). Comparison of the performance of multi-layer perceptron and linear regression for epidemiological data. *Computational Statistics & Data Analysis*, *44*(4), 547–570. https://doi.org/10.1016/S0167-9473(02)00257-8

Gillenwater, D., Granata, T., & Zika, U. (2006). GIS-based modeling of spawning habitat suitability for walleye in the Sandusky River, Ohio, and implications for dam removal and river restoration. *Ecological Engineering*, *28*(3), 311–323. https://doi.org/10.1016/j.ecoleng.2006.08.003

Google Earth Engine. (2023). Retrieved from https://earthengine.google.com

Green, J. C. (2005). Modelling flow resistance in vegetated streams: Review and development of new theory. *Hydrological Processes*, *19*(6), 1245–1259. https://doi.org/10.1002/hyp.5564

Greenwell, B. M. (2017). pdp: An R Package for constructing partial dependence plots. *The R Journal*, *9*(1), 421. https://doi.org/10.32614/RJ-2017-016

Heldmyer, A., Livneh, B., McCreight, J., Read, L., Kasprzyk, J., & Minear, T. (2022). Evaluation of a new observationally based channel parameterization for the National Water Model. *Hydrology and Earth System Sciences*, *26*(23), 6121–6136. https://doi.org/10.5194/hess-26-6121-2022

Hengl, T. (2018). Sand content in % (kg/kg) at 6 standard depths (0, 10, 30, 60, 100 and 200 cm) at 250 m resolution. [dataset]. *Zenodo*. https://doi.org/10.5281/zenodo.2525662

Hilker, N., Badoux, A., & Hegg, C. (2009). The Swiss flood and landslide damage database 1972–2007. *Natural Hazards and Earth System Sciences*, *9*(3), 913–925. https://doi.org/10.5194/nhess-9-913-2009

Hoffimann, J., Zortea, M., De Carvalho, B., & Zadrozny, B. (2021). Geostatistical learning: Challenges and opportunities. *Frontiers in Applied Mathematics and Statistics*, *7*. https://doi.org/10.3389/fams.2021.689393

Homer, C., Dewitz, J., Yang, L., Jin, S., Danielson, P., Xian, G., et al. (2015). Completion of the 2011 national land cover database for the conterminous United States—Representing a decade of land cover change information. *Photogrammetric Engineering & Remote Sensing*, *81*, 346–354. https://doi.org/10.14358/PERS.81.5.345

Hu, K., Wu, C., Wei, L., Zhang, X., Zhang, Q., Liu, W., & Yanites, B. J. (2021). Geomorphic effects of recurrent outburst superfloods in the Yigong River on the southeastern margin of Tibet. *Scientific Reports*, *11*(1), 15577. https://doi.org/10.1038/s41598-021-95194-1

Ippolito, P. P. (2022). Hyperparameter tuning. In R. Egger (Ed.), *Applied data science in tourism: Interdisciplinary approaches, methodologies, and applications* (pp. 231–251). Springer International Publishing. https://doi.org/10.1007/978-3-030-88389-8_12

James, C. S. (1994). Evaluation of methods for predicting bend loss in meandering channels. *Journal of Hydraulic Engineering*, *120*(2), 245–253. https://doi.org/10.1061/(ASCE)0733-9429(1994)120:2(245)

Jarrett, R. D. (1985). *Determination of roughness coefficients for streams in Colorado*. U.S. Department of the Interior, Geological Survey.

Ji, X., Lesack, L. F. W., Melack, J. M., Wang, S., Riley, W. J., & Shen, C. (2019). Seasonal and Interannual patterns and controls of hydrological fluxes in an Amazon floodplain lake with a surface-subsurface process model. *Water Resources Research*, *55*(4), 3056–3075. https://doi.org/10.1029/2018WR023897

Keulegan, G. H. (1938). Laws of turbulent flow in open channels. *Journal of Research of the National Bureau of Standards*, *21*(6), 707. https://doi.org/10.6028/jres.021.039

Knighton, D. (1989). *Fluvial forms and processes: A new perspective*. Routledge & CRC Press. Retrieved from https://www.routledge.com/Fluvial-Forms-and-Processes-A-New-Perspective/Knighton/p/book/9780340663134

Kundzewicz, Z. W., Hegger, D. L. T., Matczak, P., & Driessen, P. P. J. (2018). Flood-risk reduction: Structural measures and diverse strategies. *Proceedings of the National Academy of Sciences*, *115*(49), 12321–12325. https://doi.org/10.1073/pnas.1818227115

Langendoen, E. J., & Simon, A. (2008). Modeling the evolution of incised streams. II: Streambank erosion. *Journal of Hydraulic Engineering*, *134*(7), 905–915. https://doi.org/10.1061/(ASCE)0733-9429(2008)134:7(905)

Li, H.-Y., Leung, L. R., Getirana, A., Huang, M., Wu, H., Xu, Y., et al. (2015). Evaluating global streamflow simulations by a physically based routing model coupled with the community land model. *Journal of Hydrometeorology*, *16*(2), 948–971. https://doi.org/10.1175/jhm-d-14-0079.1

Li, Y., Anim, D. O., Wang, Y., Tang, C., Du, W., Yu, Z., & Acharya, K. (2014). An open-channel flume study of flow characteristics through a combined layer of submerged and emerged flexible vegetation. *Ecohydrology*, *7*(2), 633–647. https://doi.org/10.1002/eco.1384

Lin, P., Pan, M., Beck, H. E., Yang, Y., Yamazaki, D., Frasson, R., et al. (2019). Global reconstruction of naturalized river flows at 2.94 million reaches. *Water Resources Research*, *55*(8), 6499–6516. https://doi.org/10.1029/2019WR025287

Mabbott, R., & Fryirs, K. (2022). Geomorphic and vegetative river recovery in a small coastal catchment of New South Wales, Australia: Implications for flow hydrology and river management. *Geomorphology*, *413*, 108334. https://doi.org/10.1016/j.geomorph.2022.108334

Mangukiya, N. K., & Yadav, S. M. (2022). Integrating 1D and 2D hydrodynamic models for semi-arid river basin flood simulation. *International Journal of Hydrology Science and Technology*, *14*(2), 206–228. https://doi.org/10.1504/IJHST.2022.124549

Manning, R., Griffith, J. P., Pigot, T. F., & Vernon-Harcourt, L. F. (1890). *On the flow of water in open channels and pipes*. Transactions of the Institution of Civil Engineers.

Mays, L. (2019). *Water resources engineering* (3rd ed.). Wiley. Retrieved from https://www.wiley.com/en-us/Water+Resources+Engineering%2C+3rd+Edition-p-9781119490579

Mehedi, M. A. A., Smith, V., Hosseiny, H., & Jiao, X. (2022). Unraveling the complexities of urban fluvial flood hydraulics through AI. *Scientific Reports*, *12*(1), 18738. Article 1. https://doi.org/10.1038/s41598-022-23214-9

Mi, X., Zou, B., Zou, F., & Hu, J. (2021). Permutation-based identification of important biomarkers for complex diseases via machine learning models. *Nature Communications*, *12*(1), 3008. https://doi.org/10.1038/s41467-021-22756-2

Mohanta, A., Patra, K. C., & Sahoo, B. B. (2018). Anticipate Manning's coefficient in meandering compound channels. *Hydrology*, *5*(3), 47. Article 3. https://doi.org/10.3390/hydrology5030047

Naghavi, M., Mohammadi, M., & Mahtabi, G. (2023). The effect of building arrangement on the flow characteristics in meandering compound channels. *Journal of Environmental Management*, *331*, 117288. https://doi.org/10.1016/j.jenvman.2023.117288

NHD Plus. (2023). NHDPlus version 2. Retrieved from https://nhdplus.com/NHDPlus/NHDPlusV2_home.php

Nicosia, A., & Ferro, V. (2023). Flow resistance due to shrubs and woody vegetation. *Flow Measurement and Instrumentation*, *89*, 102308. https://doi.org/10.1016/j.flowmeasinst.2023.102308

Noarayanan, L., Murali, K., & Sundar, V. (2012). Manning's 'n' co-efficient for flexible emergent vegetation in tandem configuration. *Journal of Hydro-Environment Research*, *6*(1), 51–62. https://doi.org/10.1016/j.jher.2011.05.002

Pradhan, A., & Khatua, K. K. (2018a). Assessment of roughness coefficient for meandering compound channels. *KSCE Journal of Civil Engineering*, *22*(5), 2010–2022. https://doi.org/10.1007/s12205-017-1818-9

Pradhan, A., & Khatua, K. K. (2018b). Gene expression programming to predict Manning's *n* in meandering flows. *Canadian Journal of Civil Engineering*, *45*(4), 304–313. https://doi.org/10.1139/cjce-2016-0569

Rajib, A., Liu, Z., Merwade, V., Tavakoly, A. A. & Follum, M. L. (2020). Towards a large-scale locally relevant flood inundation modeling framework using SWAT and LISFLOOD-FP. *Journal of Hydrology*, *581*, 124406. https://doi.org/10.1016/j.jhydrol.2019.124406

Richardson, E. V., & Davis, S. R. (2001). *Evaluating scour at bridges [Fourth Edition] (FHWA-NHI-01-001)*. U.S. National Highway Institute & U.S. Federal Highway Administration, Office of Bridge Technology. Retrieved from https://rosap.ntl.bts.gov/view/dot/50281

Roushangar, K., & Shahnazi, S. (2021). Insights into the prediction capability of roughness coefficient in current ripple bedforms under varied hydraulic conditions. *Journal of Hydroinformatics*, *23*(6), 1182–1196. https://doi.org/10.2166/hydro.2021.161

Rowiński, P. M., Okruszko, T., & Radecki-Pawlik, A. (2022). Environmental hydraulics research for river health: Recent advances and challenges. *Ecohydrology and Hydrobiology*, *22*(2), 213–225. https://doi.org/10.1016/j.ecohyd.2021.12.003

Salleh, M. Z. M., Ibrahim, Z., Saari, R., Mohd Shariff, M. E., & Jumain, M. (2023). In S. Harun, I. K. Othman, & M. H. Jamal (Eds.), *The influence of vegetated alternate bar on flow resistance in an Alluvial Straight channel. In Lecture Notes in Civil engineering. Proceedings of the 5th international conference on water resources (ICWR) – volume 1* (pp. 167–176). Springer Nature. https://doi.org/10.1007/978-981-19-5947-9_14

Schwarz, G. E., Jackson, S. E., & Wieczorek, M. E. (2018a). Select attributes for NHDPlus version 2.1 reach catchments and modified network routed upstream watersheds for the conterminous United States. [dataset]. *U.S. Geological Survey*. https://doi.org/10.5066/F7765D7V

Schwarz, G. E., Jackson, S. E., & Wieczorek, M. E. (2018b). Select attributes for NHDPlus version 2.1 reach catchments and modified network routed upstream watersheds for the conterminous United States. [dataset]. *U.S. Geological Survey*. https://doi.org/10.5066/F7765D7V

Shen, C., Riley, W. J., Smithgall, K. R., Melack, J. M., & Fang, K. (2016). The fan of influence of streams and channel feedbacks to simulated land surface water and carbon dynamics. *Water Resources Research*, *52*(2), 880–902. https://doi.org/10.1002/2015WR018086

Singh, V. P. *Handbook of applied hydrology*, 2nd ed. (2017). McGraw-Hill Education—Access Engineering. Retrieved from https://www.accessengineeringlibrary.com/content/book/9780071835091

Song, Y., Liang, J., Lu, J., & Zhao, X. (2017). An efficient instance selection algorithm for k nearest neighbor regression. *Neurocomputing*, *251*, 26–34. https://doi.org/10.1016/j.neucom.2017.04.018

Trabucco, A., & Zomer, R. (2019). Global aridity index and potential evapotranspiration (ET0) climate database V2. [dataset]. *Figshare*. https://doi.org/10.6084/m9.figshare.7504448.v3

U.S. Geological Survey. (2023). National Hydrography dataset. [dataset]. Retrieved from https://www.usgs.gov/national-hydrography/national-hydrography-dataset

Vashist, K., & Singh, K. K. (2022). Improvement in 1D hydrodynamic modeling using MIKE Hydro. *Modeling Earth Systems and Environment*, *8*(4), 5653–5663. https://doi.org/10.1007/s40808-022-01437-z

Waliser, D., & Guan, B. (2017). Extreme winds and precipitation during landfall of atmospheric rivers. *Nature Geoscience*, *10*(3), 179–183. Article 3. https://doi.org/10.1038/ngeo2894

Yamazaki, D., Kanae, S., Kim, H., & Oki, T. (2011). A physically based description of floodplain inundation dynamics in a global river routing model. *Water Resources Research*, *47*(4). https://doi.org/10.1029/2010WR009726

Yang, F., Wu, J., Zhang, Y., Zhu, S., Liu, G., Chen, G., et al. (2021). Improved method for identifying Manning's roughness coefficients in plain looped river network area. *Engineering Applications of Computational Fluid Mechanics*, *15*(1), 94–110. https://doi.org/10.1080/19942060.2020.1858967

Yaryan Hall, H. R., & Bledsoe, B. P. (2023). Integrating channel design and assessment methods based on sediment transport capacity in gravel bed streams. *JAWRA Journal of the American Water Resources Association*, *59*(4), 681–700. https://doi.org/10.1111/1752-1688.13108

Ye, A., Zhou, Z., You, J., Ma, F., & Duan, Q. (2018). Dynamic Manning's roughness coefficients for hydrological modelling in basins. *Hydrology Research*, *49*(5), 1379–1395. https://doi.org/10.2166/nh.2018.175

Zhu, X., Liu, B., & Liu, Y. (2020). New method for estimating roughness coefficient for Debris flows. *Water*, *12*(9), 2341. Article 9. https://doi.org/10.3390/w12092341